An evaluation of the general composition and critical raw material content of bauxite residue in a storage area over a twelve-year period

Patricia B. Cusack[a,b], Ronan Courtney[a,b], Mark G. Healy[c], Lisa M. T. O' Donoghue[d], Éva Ujaczki[b,d,e*]

[a]Department of Biological Sciences, University of Limerick, Castletroy, Co. Limerick, Ireland.

[b]The Bernal Institute, University of Limerick, Castletroy, Co. Limerick, Ireland.

[c]Civil Engineering, National University of Ireland, Galway, Ireland.

[d]School of Engineering, University of Limerick, Castletroy, Co. Limerick, Ireland.

[e]Department of Applied Biotechnology and Food Science, Faculty of Chemical Technology and Biotechnology, Budapest University of Technology and Economics, Műegyetem rkp. 3, 1111 Budapest, Hungary.

*Corresponding Author: Éva Ujaczki

E-mail address: eva.ujaczki@ul.ie

Highlights

- The composition of stored bauxite residue was examined in a residue disposal area.
- Bauxite residue critical raw material content did not vary over time in storage.
- The pH of the bauxite residue in storage ranged from 10 ± 0.1 to 12.0 ± 0.02 .
- The gallium content measured in the bauxite residue was 107 ± 7.3 mg kg^{-1}.

Abstract

Bauxite residue, the by-product produced in the alumina industry, is being produced at an estimated global rate of approximately 150 million tonnes per annum. Currently, the reuse of bauxite residue is low (~ 2%), due to limitations associated with its alkalinity, salinity, low solid content, fine particle size and potential leaching of metal(loid)s. It has been identified as a potential secondary source for critical raw materials such as vanadium, gallium and scandium, which currently have an associated supply risk and high economic cost within Europe. However, there is an uncertainty regarding the possible variation in these and other physico-chemical, elemental and mineralogical parameters within bauxite residue disposal areas. This paper aimed to address this knowledge gap by examining the variation of these parameters in a bauxite residue disposal area (BRDA) over a twelve-year period. The general composition did not vary greatly within the bauxite residue examined, with the exception of pH and electrical conductivity, which ranged from 10 ± 0.1 to 12.0 ± 0.02 and from 0.4 ± 0.01 to 3.3 ± 0.2 mS cm^{-1}, respectively. The bauxite residue contained critical raw materials, of which the amount of vanadium, gallium and scandium did not vary significantly over time. The vanadium and gallium were present in larger amounts compared to other European bauxite residues. On average the vanadium, gallium and scandium content measured in the bauxite residue samples were 510 ± 77.8, 107 ± 7.3 and 51.4 ± 5.4 mg kg^{-1}, respectively. This shows promise for the potential reuse of bauxite residue as a secondary source for critical raw materials and also indicates that BRDAs may be potential mines for critical raw material extraction.

Keywords: bauxite residue, bauxite residue disposal area, reuse value, critical raw materials

Nomenclature

Al	aluminium
AlO(OH)	boehmite
$Al(OH)_3$	aluminium hydroxide hydrate
Al_2O_3	aluminium oxide
As	arsenic
BRDA(s)	bauxite residue disposal area(s)
Bt	billion tonnes
CaO	calcium oxide
$Ca(OH)_2$	slaked lime
$CaTiO_3$	perovskite
Cd	cadmium
Ce	cerium
Co	cobalt
CO_2	carbon dioxide
CRM(s)	critical raw material(s) (mg kg^{-1})
Cr	chromium
Cu	copper
DSC	differential scanning calorimetry (mW)
Dy	dysprodium
EC	electrical conductivity (mS cm^{-1})
EDS	energy-dispersive x-ray spectroscopy (weight %)
Er	erbium
Eu	europium
EU	European Union

77	Fe	iron
78	FeO(OH)	goethite
79	Fe_2O_3	iron oxide
80	Ga	gallium
81	Gd	gadolinium
82	HCl	hydrochloric acid
83	HNO_3	nitric acid
84	Ho	holmium
85	ICP-OES	inductively coupled plasma optical emission spectrometer
86	In	indium
87	Kα	k alpha
88	kV	kilovolt
89	La	lanthanum
90	Lu	lutetium
91	1M	1 molar
92	mA	milliamp
93	Mo	molybdenum
94	MPa	megapascal
95	Mt	million tonnes
96	N	nitrogen
97	NaOH	sodium hydroxide
98	Nd	neodymium
99	Ni	nickel
100	P	phosphorus
101	ρ_b	bulk density (g cm^{-3})

102	PGM	platinum group metals
103	PVDF	polyvinylidene difluoride
104	pH	pH (pH unit)
105	Pr	praseodymium
106	PSA	particle size analysis (µm and in % of the total particle distribution)
107	REE(s)	rare earth element(s) (mg kg^{-1})
108	REO(s)	rare earth oxide(s)
109	Sc	scandium
110	SEM	scanning electron microscope (µm)
111	SiO_2	silicon oxide
112	Sm	samarium
113	Tb	terbium
114	TGA	thermogravimetric analysis (mg)
115	Ti	titanium
116	TiO_2	titanium oxide
117	Tm	thulium
118	Tn	terbium
119	V	vanadium
120	XRD	x-ray diffraction (°2Θ)
121	XRF	x-ray fluorescence (%)
122	Y	yttrium
123	Yb	ytterbium
124		
125		

126 **1. Introduction**

Bauxite residue (red mud) is the by-product generated during the extraction of alumina from bauxite ore using the Bayer Process (Kirwan *et al.* 2013), and is currently being produced at a global rate of 150 Mt per annum, adding to the 3 Bt already in storage worldwide (Evans 2016). Currently, less than 2 % of the bauxite residue generated annually is being reused (Ujaczki *et al.* 2018), with the remaining ~ 98 % going into bauxite residue disposal areas (BRDAs) (Burke *et al.* 2013). The average cost of disposing and managing of bauxite residue in storage is 1-2 % of the alumina price for the alumina refinery (Tsakiridis *et al.* 2004).

Current best practice guidelines for the storage of bauxite residue is to use dry-stacking, a method which involves the thickening of the bauxite residue slurry from the Bayer process, using a filter press or vacuum filtration (depending on the refinery), before being spread in layers in the BRDA (Power *et al.* 2011; Evans 2016). Depending on the nature of the bauxite ore used, some refineries operate a separation technique (Evans 2016), which allows the bauxite residue to be separated into two main size fractions: a fine fraction (particle size <100 µm) and a coarse fraction (particle size > 150 µm) (IAI 2015; Jones *et al.* 2012). Bauxite residue is typically characterised as being highly alkaline, saline and composed of mainly fine particles comprised of a wide range of metal(loid)s and minerals (Gräfe *et al.* 2009). This poses challenges in the long-term management of BRDAs in terms of protecting the surrounding environment (Higgins *et al.* 2017; Kong *et al.* 2017), due to the high alkalinity, increased risk of dust pollution (due to the fine particles), and leaching of trace elements (Wang *et al.* 2015; Kong *et al.* 2017). The disposal conditions and management of residue in a BRDA is dependent on many factors such as location, climate, engagement with local communities and stakeholders (IAI 2015) and involves licencing permits from regulatory

152 authorities (such as the Environmental Protection Agency). For example, European operators
153 must meet the requirements according to the European List of Waste and Directive (EU
154 Communities 1999, 2002). As a result of this, some refineries implement neutralisation
155 techniques prior to disposal, such as carbon dioxide (CO_2) sparging of residues (Cooling
156 2007) or post disposal through the use of atmospheric carbonation (mud farming) with
157 amphirolling (Evans 2016) in the BRDA, which helps in the neutralisation, dewatering and
158 compaction of the bauxite residue (Evans 2016; Gomes *et al.* 2016; Higgins *et al.* 2016; Zhu
159 *et al.* 2016), reducing both alkalinity and moisture content, which are two limitations to the
160 re-use of bauxite (Evans 2016).
161
162 Traditionally, the reuse of bauxite residue has focussed on construction applications such as
163 cementitious application (Pontikes and Angelopoulos 2013; Nikbin *et al.* 2018). Some other
164 reuse options for bauxite residue have included polymers (Hertel *et al.* 2016), ceramics
165 (Pontikes *et al.* 2009) and catalysts (Wang *et al.* 2008); adsorbents for wastewater treatment
166 (Bhatnagar *et al.* 2011), particularly for the removal of arsenic (As) (Arco-Lázaro *et al.*
167 2018), chromium (Cr) (Dursun *et al.* 2008), nickel (Ni) (Hannachi *et al.* 2010), copper (Cu)
168 (Atasoy and Bilgic 2018), cadmium (Cd) (Ha *et al.* 2017) and phosphorus (P) (Cusack *et al.*
169 2018), as well as applications as potential soil ameliorants (Ujaczki *et al.* 2015). More
170 recently and due to the demand of critical raw materials (CRMs), particularly the rare earth
171 elements (REEs), studies have examined the potential of bauxite residue as a secondary
172 source of these materials and their potential economic value (Gomes *et al.* 2016; Xue *et al.*
173 2016; Ujaczki *et al.* 2017).
174
175 Within the European Union (EU), the 'Raw Materials Initiative' ensures that Europe secures
176 and sustains an affordable supply of CRMs which are identified as being of high economic

177 importance and having a risk to their supply (EU COM/2017/0490). The list of 27 CRMs
178 features elemental groups and single elements, including platinum group metals (PGM) and
179 REEs (EU COM/2017/0490). The REEs are divided into light REE [lanthanum (La), cerium
180 (Ce), praseodymium (Pr), neodymium (Nd), samarium (Sm), europium (Eu)] and heavy REE
181 [gadolinium (Gd), terbium (Tb), dysprodium (Dy), holmium (Ho), erbium (Er), thulium
182 (Tm), ytterbium (Yb), lutetium (Lu), including yttrium (Y)] (Xu *et al.* 2017) plus scandium
183 (Sc) (Binnemans *et al.* 2018). Depending on the origin of the bauxite residue generated, it
184 may be a potentially valuable source of CRM and other elements e.g. REEs, Sc, V, Ga, and
185 titanium (Ti) (Liu and Naidu 2014). Also included in the 2017 CRM list is P and phosphate
186 rock, which are also of particular interest, as bauxite residue has been previously identified as
187 having a high P retention capacity (Grace *et al.* 2015, 2016; Cusack *et al.* 2018) due to its
188 high aluminium (Al) and iron (Fe) oxide content (IAI 2015), making it a possible resource in
189 the removal and recovery of P from aqueous solutions (Grace *et al.* 2015; Cusack *et al.*
190 2018).
191
192 Although bauxite residues are typically similar in composition, properties can vary between
193 refineries and this is attributed to the type of ore used, as well as different process parameters,
194 such as temperature, pressure and concentrations of caustic soda (NaOH), slaked lime
195 ($Ca(OH)_2$) and other additives used in the Bayer process (Gräfe *et al.* 2009; Gräfe *et al.*
196 2011). This indicates that re-use options should be refinery-specific (Balomenos *et al.* 2017).
197 A further potential limitation, is that bauxite residue composition, such as pH and bulk
198 density, may change over time in storage (Kong *et al.* 2017a; Zhu *et al.* (2016a,b), which
199 greatly influences the possibility of reusing bauxite residue.
200

To date, no study has investigated the CRM content variability in bauxite residue stored within one specific BRDA. Therefore, the objectives of this study were to: (1) characterise the physico-chemical, elemental and mineralogical composition of the dominant fraction (fine fraction) bauxite residue in storage over a twelve-year period, and to determine if there is any variation over the time spent in storage, which could affect possible reuse of the bauxite residue (2) create an inventory of economically interesting elements in bauxite residue over the storage period, and (3) calculate the financial value of economically interesting elements present in the bauxite residue.

2. Materials and Methods

2.1 Site description and sample collection

Bauxite residue was obtained from a European refinery, who operated a separation technique to isolate the fine (particle sizes <100 μm) and coarse (particle sizes >150 μm) fractions of bauxite residue before disposal (IAI 2015), in an approximate ratio of 9:1 (fine: coarse). Bauxite residue was sampled to a depth of 30 cm and the bulk samples were stored in 1 L containers, returned to the laboratory, and dried at 105˚C for 24 hr. Once dry, the samples were pulverised using a mortar and pestle and sieved to a particle size < 2 mm. In this paper, the age of the samples will be described (Table 1) relative to the sample collection time (2016).

221 2.2 Characterisation Study

222 2.2.1 Physico-chemical composition

223 The bauxite residue samples were characterised (n=3) for their physical, chemical, elemental
224 and mineralogical properties (Figure 1). The pH and electrical conductivity (EC) were
225 measured using a 5 g sample in an aqueous extract, using a 1:5 ratio (solid: liquid) (Courtney
226 and Harrington, 2010). The bulk density (ρ_b) was determined after Blake (1965), the
227 effective particle size analysis (PSA) was determined on particle sizes < 53 μm using optical
228 laser diffraction on a Malvern Zetasizer 3000HS® (Malvern, United Kingdom) with online
229 autotitrator and a Horiba LA-920, and reported at specific cumulative % (10, 50 and 90 %).
230 Thermogravimetric analysis (TGA) was carried out to identify any change in mass over time
231 with temperature, and change in heat flow over time with temperature was analysed using
232 differential scanning calorimetry (DSC). TGA and DSC were carried performed using a
233 Labsys TG (DSC/TGA 1600) in a nitrogen (N) atmosphere at a temperature range of 30 °C to
234 1000 °C at a heating rate of 10 °C min^{-1} (Borra *et al*. 2015). Due to cost limitations, only six
235 samples were analysed (BR12, BR10, BR8, BR6, BR4 and BR2).

236

237 2.2.2 Mineralogical composition

238 Mineralogical detection was carried out on 1 g powdered samples using X-ray diffraction
239 (XRD) on a Philips X'Pert PRO MPD® (California, USA) at 40 kV, 40 mA, 25 °C by Cu X-
240 ray tube (Kα-radiation). The patterns were collected in the angular range from 5 to 80 º (2ɵ)
241 with a step-size of 0.008 º (2ɵ) (Castaldi *et al.* 2011), whilst surface morphology and
242 elemental detection were carried out using scanning electron microscopy (SEM) and energy-
243 dispersive X-ray spectroscopy (EDS) on a Hitachi SU-70 (Berkshire, UK). X-ray
244 fluorescence (XRF) analysis was carried out onsite at the refinery using a Panalytical Axios
245 XRF (Malvern, UK).

246

247 2.2.3 Elemental composition

248 Chemical analysis of minor elements was performed after aqua regia digestion (HCl: HNO_3)
249 with a solid to liquid ration of 1:10 in a Multiwave 3000 (Rotor 8XF100) type microwave
250 digestion system at 200 °C 1.25 MPa. After digestion, the solutions were filtered through
251 0.45 µm PVDF syringe filters and diluted in 1 M HNO_3 for the analysis (Ujaczki *et al.* 2017).
252 The metal analysis was carried out using an Agilent Technologies 5100 inductively coupled
253 plasma optical emission spectrometer (ICP-OES). The calibration curve was constructed
254 using standard solutions of 100, 50, 10, 5 and 1 g L^{-1} multi-element standard (Inorganic
255 Ventures, Ireland) and 5, 2.5, 0.5, 0.25 and 0.05 g L^{-1} REE standard (Inorganic Ventures,
256 Ireland). The 1M HNO_3 solution was also used for the dilutions of the standard solutions and
257 as a calibration blank. For the ICP-OES analysis, the following analytical lines (in nm) were
258 used for the calculations of each of the elements: Ce 418.659, 446.021; cobalt (Co) 228.615,
259 230.786; Dy 353.171; Er 349.910, 369.265; Eu 397.197, 412.972, 420.504; Ga 294.363; Gd
260 335.048, 336.224; Ho 339.895, 345.600, 389.094; indium (In) 230.606, 352.609; La 333.749,
261 379.477, 408.671; Lu 261.541, 307.760; molybdenum (Mo) 202.032, 203.846, 204.598; Nd
262 401.224, 406.108, 410.945; Pr 390.843, 417.939; Sc 335.372, 361.383, 363.074; Sm 359.259,
263 360.949; Tb 350.914,367.636; Tm 313.125, 342.508; Y 360.074, 371.029, 377.433; Yb
264 289.138, 328.937, 369.419; V 268.796, 292.401, 311.070 (Bridger and Knowles, 2000).

265

266 2.3 Statistical Analysis

267 Pearson's correlation coefficients were used to determine any relationships between age of
268 sample and sample properties (pH, EC, bulk density, particle size, mineralogical composition
269 and elemental composition), using IBM SPSS Statistics 24.

270

3. Results

3.1 Physico-chemical composition

The pH of the bauxite residue (Table 2) ranged from 10.0 ± 0.1 to 12.0 ± 0.02 over the twelve-year period, with the ten-year-old sample (BR10) having the highest value. The EC (Table 2) of the bauxite residue ranged from 0.4 ± 0.01 to 3.3 ± 0.2 mS cm^{-1}, with again, the highest being for BR10. Small variation in the moisture content (Table 2) for the each of the bauxite residues was recorded. The bulk density (Table 2) for the bauxite residue ranged from 1.2 ± 0.1 to 1.5 ± 0.02 g cm^{-3}.

The bauxite residue had a high composition of fine particles, which ranged from 0.6 ± 0.01 to 12.7 ± 2.3 µm (Table 2). There was some agglomerate formation evident in all samples, as seen in the accumulation of finer particles in the images captured by SEM (Figure S1, S2, S3 in the Supplementary Information). The medium value, d_{50}, of the particle size distribution for bauxite residues ranged from 2.2 ± 0.1µm (BR1) to 4.3 ± 0.4 µm (BR9). Ninety percent of the distribution (d_{90}) was under 12.7 ± 2.7 µm and 10 % (d_{10}) was under 0.5 ± 0.01 µm (Table 2). Iron, Al, sodium (Na), calcium (Ca), titanium (Ti), and silicon (Si) were the main elements present in all the bauxite residue samples (Figure S4). TGA curves showed weight loss between 300 and 975 °C for all the bauxite residues (Figures 2 and S5). However, sample BR12 (from 2014) had a larger temperature range over which weight loss occurred (between 150 and 975 °C).

3.1.1 Mineralogical Composition

The main mineralogical composition of the bauxite residue detected by XRD included haematite (Fe_2O_3), goethite ($FeO(OH)$), perovskite ($CaTiO_3$), rutile (TiO_2), gibbsite $Al(OH)_3$, sodalite ($Na_8(Al_6Si_6O_{24})Cl_2$) and cancrinite ($Na_6Ca_2(CO_3)$) (Figure S6 and S7). Sample BR9 had an extra rutile peak at position 27.459 °2Θ and no sodalite peak at position 14 °2Θ; samples BR1 to BR6 had similar patterns, but with less intense peaks and sodalite peaks at position 14 °2Θ (Figure S6). Sample BR1 had one peak of boehmite ($AlO(OH)$) at position 13.9 °2Θ and gibbsite at position 18.5 °2Θ (Figure S6). Sample BR1 also had an unidentified peak at position 47 °2Θ (Figure S6).

XRF analysis carried out on the bauxite residue samples (Table 3) reflected the main mineralogical composition detected by XRD analysis. The dominant oxides found were Fe_2O (ranging from 40.1 ± 1.40 to 47.5 ± 2.0 %) and Al_2O_3 (14.8 ± 1.5 to 17.8 ± 0.73 %). SiO_2 (7.20 ± 1.0 to 10.9 ± 0.47 %), TiO_2 (8.62 ± 0.71 to 10.3 ± 0.95 %) and CaO (5.70 ± 0.66 to 6.1 ± 1.0%) were also present (Table 3).

3.1.2 Elements of economic importance in bauxite residue

An extensive inventory of CRMs and further elements of economic importance were developed using microwave-assisted aqua regia digestion, with subsequent ICP-OES analysis (Table 4). Overall, no trend was noted in the elemental content between the oldest and newest bauxite residue in the BRDA. However, In, Mo, Ce, Nd, Dy and Er were present in smaller amounts in the oldest samples compared to the fresh sample. Terbium (Tb), Tm and Ho were not detected in the bauxite residue.

4. Discussion

4.1 Characterisation of bauxite residue

Bauxite residue typically has a pH >10 (Goloran *et al.* 2013) and an EC ranging from 1.4 to 28.4 mS cm^{-1} (Gräfe *et al.* 2011). The high pH is attributed to the presence of alkaline anions such as hydroxides (OH^-), carbonate or bicarbonates (CO_3^{2-} / HCO_3^-), aluminates or aluminium hydroxides ($Al(OH)_4^-$ / $Al(OH)_3$), and di/trihydrogen orthosilicates ($H_2SiO_4^{2-}$ / $H_3SiO_4^-$) introduced and formed during the Bayer process (Gräfe *et al.* 2011). At the end of the Bayer process, prior to disposal, residue undergoes a repeated washing stage. However, the bauxite residue remains highly alkaline due to the alkalinity being in the form of slow dissolving solid phases (Gräfe *et al.* 2011).

Depending on the refinery and the advances in residue management steps employed, the pH may be further reduced through practices such as atmospheric carbonation (mud farming) (Clohessy 2015; Evans 2016), seawater disposal (Menzies *et al.* 2009), application of spent acid (Kirwan *et al.* 2013), phosphogypsum (Xue *et al.* 2018), or by the addition of an acidic gas such as CO_2 or SO_2 (Xue *et al.* 2016). Consequently, surface pH values for residues may vary between refineries and within BRDAs.

The bauxite residue examined in this study showed variation in terms of both the pH and the EC ($p < 0.01$) (Table 2). Whilst the pH and EC did decrease across all the bauxite residue samples examined in this study (Table 2), this was attributed to different causes. The reduced pH value of the fresh bauxite residue examined (BR1) in this study (Table 2) is as a result of the atmospheric carbonation technique, mud farming, which can effectively decrease alkalinity (Clohessy 2015; McMahon 2017). This helps in removing the alkalinity

limitation/barrier to the reutilisation of the bauxite residue (Evans 2016) and has been shown to successfully decrease the pH of fresh bauxite residue (~ 13.5) to below < 11.5 within seven days (Clohessy 2015). The mud farming technique sequesters CO_2 from the atmosphere, allowing for the accelerated carbonation of the bauxite residue (IAI 2015; Evans 2016). Due to this process, the free OH^- present in the bauxite residue is neutralised due to the carbonation of the CO_2 present in the surrounding atmosphere (air), resulting in the formation of carbonates, therefore creating a buffering effect, which results in a drop in pH (Han *et al.* 2017).

Natural weathering processes may play an important role in the improvement of the physico-chemical composition of bauxite residue in storage (Zhu *et al.* 2018). The reduction observed in the pH of the older samples (Table 2) is as a result of the natural ageing and weathering of the bauxite residue in storage. Evidence of the natural weathering decreasing the pH was shown by Khaitan *et al.* (2010), who reported a pH of 10.5 for 14-year-old bauxite residue and 9.5 for 35-year-old bauxite residue, with the decreases attributed to the slow carbonation from atmospheric CO_2. Zhu *et al.* (2016a,b) also measured a decrease in residue pH from 10.98 to 9.45 in stored bauxite residue exposed to natural weathering processes. Similar to pH, EC usually decreases with time in the storage area due to weathering (Zhu *et al.* 2016a,b; Kong *et al.* 2017a). Rainfall events allow the soluble alkaline minerals such as sodalite and calcite, which result in a buffering effect for both pH and salinity (EC) (Santini and Fey, 2013).

The thermal analysis (TGA/DSC) indicated an overall weight loss occurring between 300 and 975 °C for all the bauxite residue samples examined. Previous work has shown weight loss between temperature ranges of 300 and 600 °C (attributed to the decomposition of

hydroxides in different stages), 300 and 400 °C (as a result of the decomposition of diaspora), and between 600 and 800 °C (due to the decomposition of calcium carbonate) (Agatzini-Leonardou *et al.* 2008), all dominant minerals in bauxite residue. There were numerous endothermic peaks observed on the DSC curve for the six samples examined, particularly in the region above 800°C. Endothermic peaks above this temperature are indicative of the decomposition of sodalite phases and also the decomposition of quartz, which occurs between 550 to 1000°C (Atasoy 2005). Small endothermic peaks throughout the DSC curve may be attributed to loss of physically held water (Atasoy, 2005), which was notable in all the bauxite residue samples examined.

The mineralogical composition of bauxite residue typically comprises Al_2O_3 and Fe_2O_3 in the range of 20 to 45 % and 10 to 22 %, respectively (IAI 2015). This composition is reflected in the XRF and XRD analysis, which showed the dominant presence of Fe_2O_3, FeO(OH), and $Al(OH)_3$. $CaTiO_3$, AlO(OH) and TiO_2 were also detected in all samples, which is common amongst bauxite residue (Gräfe *et al.* 2011). Sodalite ($Na_8(Al_6Si_6O_{24})Cl_2$) was also present in the bauxite residue, and is one of the most common desilication products formed during the pre-desilication stage during the Bayer process, along with $CaTiO_3$ which is often found as a result of the lime added (Gräfe *et al.* 2011).

4.2 Economic value of bauxite and potential for reuse

In recent years, several studies have been conducted to investigate the potential use of industrial residues such as phosphogypsum, mine tailings, slags and bauxite residue as a possible source for CRMs and REEs (Binnemans *et al.* 2015). Currently, the global production rate of REEs, which is typically expressed in tons of rare earth oxides (REOs) is 130,000 to 140,000 tons, of which 95% is produced in China (Binnemans *et al.* 2018). Five

of the REEs (Nd, Eu, Tb, Dy, Y) are now described as being of a high supply risk within Europe, Japan and the USA (Binnemans *et al.* 2018). Such CRMs and REEs are necessary for the production of magnets, lighting, lasers, batteries, catalysts, and alloys in aerospace (Weng *et al.* 2015).

While this study did show differences in the bauxite residue over the twelve-year period, in terms of decreased pH and EC, there were no significant changes in the CRM content of the bauxite residue (Table 4). This indicates that some BRDAs may be a potential resource for the reprocessing and recovery of CRMs and REEs. However, this is not certain for all BRDAs, as variation can and does occur within BRDAs and refineries due to differences in bauxite ore type, parameters used within the Bayer Process, as well as varying disposal and neutralisation techniques.

The Sc, Ga and V content of the bauxite residue in the current study are of particular interest, due to their high economic value (Table 5) and supply risk. Scandium, a trace constituent of igneous rocks (European Commission, 2017), is used in the production of aluminium alloys (Ricketts and Duyvesteyn 2018), and V, present in minor amounts in the Earth's crust and seawater and the majority of which is sourced as a by-product of the steel industry (European Commission, 2017), is used in electrodes (Morel *et al.* 2016). Gallium is primarily sourced from bauxite ore and bauxite residue, as it found naturally as a trace element dispersed in minerals, which also includes coal (Qin *et al.* 2015), and is used in the production of catalysts (Qin and Schneider 2016). The Sc in this study (Table 4) was lower than values found in fresh Hungarian (Ujaczki *et al.* 2017), Greek (Borra *et al.* 2015), Russian (Petrakova *et al.* 2015) and Australian (Wang *et al.* 2013) bauxite residues. However, the Ga content (Table 4) was higher than that found by Ujaczki *et al.* (2017) in Hungarian bauxite residue, as well

as in Australian (Wang *et al.* 2013), Indian (Mohapatra *et al.* 2012) and Turkish (Abdulvaliyev *et al.* 2015) bauxite residues. Finally, the V content was present in higher amounts compared to Hungarian (Ujaczki *et al.* 2017), Indian (Mohapatra *et al.* 2012) and Turkish (Abdulvaliyev *et al.* 2015) bauxite residues. This is indicative of the variation of CRM content in residues between refineries. In addition to Sc, Ga and V, there is now a focus on further valuable element extraction (Jowitt *et al.* 2018) and recovery of REE due to the overproduction of REEs such as La and Ce, which is leading to an imbalance in the supply of REEs produced and a demand for Nd and Dy (Binnemans and Jones 2015; Binnemans *et al.* 2018), both of which were found in the bauxite residue in this study.

The typical methods of CRM recovery from bauxite residue include direct leaching using mineral acids such as HNO_3, sulphuric acid (H_2SO_4) or hydrochloric acid (HCl), or leaching following pyrometallurgical applications such as roasting (Ujaczki *et al.* 2018). Although there are high recovery rates of CRMs from bauxite residue reported (Abdulvaliyev *et al.* 2015; Borra *et al.* 2015), so too are the associated costs for acids and energy required in these processes, which questions the justification of extracting CRMs from by-products such as bauxite residue. Recent studies have also highlighted the need to develop new technologies to optimise the efficiency of CRM recovery from bauxite residue to ensure cost-effectiveness (Gomes *et al.* 2016; Akcil *et al.* 2017). Ujaczki *et al.* (2018) in their review on the reuse of bauxite residue as a source of CRMs, highlighted the extent of the benefits following CRM recovery from a wider perspective in terms of the technological (development of more efficient technologies), social (such as improvements to health), economic (mainly reduction in refinery disposal costs), and environmental factors such as reduced emissions and loss of habitable land.

440 4.3 The findings of this study from an industrial perspective on potential re-use of bauxite
441 residue
442 This study found that there was very little variation in the CRM content of bauxite residue in
443 a BRDA over a twelve-year period. This shows promise for the potential reuse of bauxite
444 residue as a secondary source of CRMs. Finding a suitable and long-term use for bauxite
445 residue may be hampered by several barriers and limitations (Klauber *et al.* 2011; Evans
446 2016), such as high alkalinity and salinity which were shown by this study to be reduced by
447 weathering and mud farming. However, limitations to the reuse of bauxite residue may be
448 overcome through management strategies involving its partial neutralisation and increased
449 solids content (Klauber *et al.* 2011).
450
451 **5. Conclusions**
452 This study showed that there was a reduction in both the pH and the EC ($p < 0.01$) of bauxite
453 residue in a BRDA over a twelve-year period. There was little variation in the CRM content
454 of the bauxite residue sampled. The CRMs of particular interest were V, Ga and Sc due their
455 potential supply risk and associated economic value. The V, Ga and Sc content of the bauxite
456 residue samples were 510 ± 77.8, 107 ± 7.3 and 51.4 ± 5.4 mg kg^{-1}, respectively, giving
457 current economic values of 3.51, 42.73 and 236.44 US \$ t^{-1}. From a European and global
458 context, this highlights a potential resource for CRMs in the event of a scarcity of these
459 materials. However, the general composition and CRM content of bauxite residue varies
460 greatly due to the bauxite ore and parameters used in the Bayer Process, as well as the
461 disposal and neutralisation methods implemented by refineries. Depending on the history of
462 the refinery and BRDA, there may be little variation over time, making BRDAs possible
463 sources for the extraction of CRMs. There are currently high-costs associated with the
464 extraction of CRMs from bauxite residue due to the large amount of reagent and/or energy

465 required in the process, before purifying the CRMs recovered for reuse. However, these need
466 to be set against the overall benefits of recovering CRMs in terms of the environmental,
467 economic and social factors. Further research is necessary to investigate the cost and
468 environmental implications and limitations of extraction of CRMs from BRDAs, as opposed
469 to conventional extraction techniques from mines, in terms of emissions produced, machinery
470 required, fuel needed and human resources required.
471

472 **Acknowledgements**

473 The authors would like to acknowledge the financial support of the Environmental Protection
474 Agency (EPA) (2014-RE-MS-1).
475

476 **References**

477 Abdulvaliyev, R.A., Akcil, A., Gladyshev, S.V., Tastanov, E.A., Beisembekova, K.O.,
478 Akhmadiyeva, N.K. and Deveci, H., 2015. Gallium and vanadium extraction from red mud of
479 Turkish alumina refinery plant: Hydrogarnet process. Hydrometallurgy 157, 72-77.
480

481 Agatzini-Leonardou, S., Oustadakis, P., Tsakiridis, P.E. and Markopoulos, C., 2008. Titanium
482 leaching from red mud by diluted sulfuric acid at atmospheric pressure. J. Hazard. Mater. 157,
483 579-586.
484

485 Akcil, A., Akhmadiyeva, N., Abdulvaliyev, R., Abhilash and Meshram, P., 2018. Overview on
486 extraction and separation of rare earth elements from red mud: focus on scandium. Mineral.
487 Process. Extract. Metall. Rev. 39,145-151.
488

Arco-Lázaro, E., Pardo, T., Clemente, R. and Bernal, M.P., 2018. Arsenic adsorption and plant availability in an agricultural soil irrigated with As-rich water: effects of Fe-rich amendments and organic and inorganic fertilisers. J. Environ. Manage. 209, 262-272.

Atasoy, A., 2005. An investigation on characterization and thermal analysis of the Aughinish red mud. J. Therm. Anal. Calorim. 81, 357-361.

Atasoy, A.D. and Bilgic, B., 2018. Adsorption of copper and zinc ions from aqueous solutions using montmorillonite and bauxite as low-cost adsorbents. Mine Wat. Environ. 37, 205-210.

Balomenos, E., Davris, P., Pontikes, Y. and Panias, D., 2017. Mud2Metal: Lessons learned on the path for complete utilization of bauxite residue through industrial symbiosis. J. Sustain. Metall. 3, 551-560.

Bhatnagar, A., Vilar, V.J., Botelho, C.M. and Boaventura, R.A., 2011. A review of the use of red mud as adsorbent for the removal of toxic pollutants from water and wastewater. Environ. Technol. 32, 231-249.

Binnemans, K. and Jones, P.T., 2015. Rare earths and the balance problem. J. Sustain. Metall. 1, 29-38.

Binnemans, K., Jones, P.T., Blanpain, B., Van Gerven, T. and Pontikes, Y., 2015. Towards zero-waste valorisation of rare-earth-containing industrial process residues: a critical review. J. Clean. Prod. 99, 17-38.

514 Binnemans, K., Jones, P.T., Müller, T. and Yurramendi, L., 2018. Rare earths and the balance
515 problem: how to deal with changing markets? J. Sustain. Metall. 4, 1-21.
516
517 Blake, G.R., 1965. Bulk Density 1. Methods of soil analysis. Part 1. Physical and mineralogical
518 properties, including statistics of measurement and sampling, (methodsofsoilana), 374-390.
519 Available:
520 https://dl.sciencesocieties.org/publications/books/tocs/agronomymonogra/methodsofsoilana
521 [accessed 24.05.2018].
522
523 Borra, C.R., Pontikes, Y., Binnemans, K. and Van Gerven, T., 2015. Leaching of rare earths
524 from bauxite residue (red mud). Minerals Engin. 76, 20-27.
525
526 Bridger, S. and Knowles, M., 2000. A complete method for environmental samples by
527 simultaneous axially viewed ICP-AES following USEPA guidelines. Varian ICP-OES At
528 Work (29). Available: https://www.agilent.com/cs/library/applications/ICPES-29.pdf
529 [accessed 24.05.2018].
530
531 Burke, I.T., Peacock, C.L., Lockwood, C.L., Stewart, D.I., Mortimer, R.J., Ward, M.B.,
532 Renforth, P., Gruiz, K. and Mayes, W.M., 2013. Behavior of aluminum, arsenic, and vanadium
533 during the neutralization of red mud leachate by HCl, gypsum, or seawater. Environ. Sci.
534 Technol. 47, 6527-6535.
535
536 Castaldi, P., Silvetti, M., Enzo, S. and Deiana, S., 2011. X-ray diffraction and thermal analysis
537 of bauxite ore-processing waste (red mud) exchanged with arsenate and phosphate. Clays and
538 Clay Min. 59, 189-199.

Clohessy, J., 2015. Closure and rehabilitation of Rusal Aughinish BRDA, presented at the Residue Closure and Rehabilitation Workshop. In 10th Alumina Quality Workshop, Perth, Western Australia. Available: (http://aqw.com.au/2015papers.html) [accessed 18.04.2018].

Cooling, D.J., 2007. Improving the sustainability of residue management practices-Alcoa World Alumina Australia. Paste and thickened tailings: a guide, 316. Available: http://citeseerx.ist.psu.edu/viewdoc/download?doi=10.1.1.629.1067&rep=rep1&type=pdf [accessed 24.05.2018].

Courtney, R. and Harrington, T., 2010. Assessment of plant-available phosphorus in a fine textured sodic substrate. Ecol. Engin. 36, 542-547.

Communication from the commission to the European Parliament, the council, the European economic and social committee and the committee of the regions, 2017. Available: http://eur-lex.europa.eu/legal-content/EN/TXT/PDF/?uri=CELEX:52017DC0490&from=EN [accessed 26.02.2018].

Cusack, P.B., Healy, M.G., Ryan, P.C., Burke, I.T., O'Donoghue, L.M., Ujaczki, É. and Courtney, R., 2018. Enhancement of bauxite residue as a low-cost adsorbent for phosphorus in aqueous solution, using seawater and gypsum treatments. J. Clean. Prod. 179, 217-224.

Dursun, S., Guclu, D., Berktay, A. and Guner, T. 2008. Removal of chromate from aqueous system by activated red-mud. Asian J. Chem. 20, 6473–6478.

564 EU Communities Commission Decision 2000/532/EC, OJ L 226, 06.09.2000; pp. 3–24.
565 Available online: http://eur-lex.europa.eu/legal-
566 content/EN/TXT/PDF/?uri=CELEX:22002D0009&from=EN [accessed 27.09.2018].
567
568 EU Communities Council Directive 1999/31/EC on the landfill of waste, OJ L 182, 16.07.1999;
569 pp. 1–19. Available online:http://eur-lex.europa.eu/legal-
570 content/EN/TXT/PDF/?uri=CELEX:31999L0031&from=EN [accessed on 27.09.2018].
571
572 European Commission, 2017. Study on the review of the list of critical raw materials. Critical
573 raw materials factsheets. Catalogue number ET-04-15-307-EN-N. Available:
574 https://publications.europa.eu/en/publication-detail/-/publication/7345e3e8-98fc-11e7-b92d-
575 01aa75ed71a1/language-en [accessed 15.05.2018].
576
577 Evans, K., 2016. The history, challenges, and new developments in the management and use
578 of bauxite residue. J. Sustain Metall. 2, 316-331.
579
580 Goloran, J.B., Chen, C.R., Phillips, I.R., Xu, Z.H. and Condron, L.M., 2013. Selecting a
581 nitrogen availability index for understanding plant nutrient dynamics in rehabilitated bauxite-
582 processing residue sand. Ecol. Engin. 58, 228-237.
583
584 Gomes, H.I., Jones, A., Rogerson, M., Burke, I.T. and Mayes, W.M., 2016. Vanadium removal
585 and recovery from bauxite residue leachates by ion exchange. Environ. Sci. Poll. Res. 23,
586 23034-23042.
587

588 Grace, M.A., Healy, M.G. and Clifford, E., 2015. Use of industrial by-products and natural
589 media to adsorb nutrients, metals and organic carbon from drinking water. Sci. Tot. Environ.
590 518, 491-497.
591
592 Grace, M.A., Clifford, E. and Healy, M.G., 2016. The potential for the use of waste products
593 from a variety of sectors in water treatment processes. J. Clean. Prod. 137, 788-802.
594
595 Gräfe, M., Power, G. and Klauber, C., 2011. Bauxite residue issues: III. Alkalinity and
596 associated chemistry. Hydrometallurgy 108, 60-79.
597
598 Ha, X.L., Hoang, N.H., Nguyen, T.T.N., Nguyen, T.T., Nguyen, T.H., Dang, V.T. and Nguyen,
599 N.H., 2017, October. Removal of Cd (II) from aqueous solutions using red mud/graphene
600 composite. In Congrès International de Géotechnique–Ouvrages–Structures (1044-1052).
601 Springer, Singapore.
602
603 Han, Y.S., Ji, S., Lee, P.K. and Oh, C., 2017. Bauxite residue neutralization with simultaneous
604 mineral carbonation using atmospheric CO2. J. Hazard. Mater. 326, 87-93.
605
606 Hannachi, Y., Shapovalov, N.A. and Hannachi, A. 2010. Adsorption of nickel from aqueous
607 solution by the use of low-cost adsorbents. Korean J. Chem. Engin. 27, 152–158.
608
609 Hertel, T., Blanpain, B. and Pontikes, Y., 2016. A proposal for a 100% use of bauxite residue
610 towards inorganic polymer mortar. J. Sustain. Metall. 2, 394-404.
611

612 Higgins, D., Curtin, T., Pawlett, M. and Courtney, R., 2016. The potential for constructed
613 wetlands to treat alkaline bauxite-residue leachate: Phragmites australis growth. Environ. Sci.
614 Poll. Res. 23, 24305-24315.
615
616 Higgins, D., Curtin, T. and Courtney, R., 2017. Effectiveness of a constructed wetland for
617 treating alkaline bauxite residue leachate: a 1-year field study. Environ. Sci. Poll. Res. 24,
618 8516-8524.
619
620 IAI, 2015. Bauxite residue management: best practice. http://www.world-
621 aluminium.org/media/filer_public/2015/10/15/bauxite_residue_management_-
622 _best_practice_english_oct15edit.pdf. [accessed: 14th October 2017].
623
624 Jones, B.E., Haynes, R.J. and Phillips, I.R., 2012. Addition of an organic amendment and/or
625 residue mud to bauxite residue sand in order to improve its properties as a growth medium. J.
626 Environ. Manage. 95, 29-38.
627
628 Jowitt, S.M., Werner, T.T., Weng, Z. and Mudd, G.M., 2018. Recycling of the rare Earth
629 elements. Curr. Opin.Green.Sustain. Chem 13, 1-7.
630
631 Khaitan, S., Dzombak, D.A., Swallow, P., Schmidt, K., Fu, J. and Lowry, G.V., 2010. Field
632 evaluation of bauxite residue neutralization by carbon dioxide, vegetation, and organic
633 amendments. J. Environ. Engin. 136, 1045-1053.
634

635 Kirwan, L.J., Hartshorn, A., McMonagle, J.B., Fleming, L. and Funnell, D., 2013. Chemistry
636 of bauxite residue neutralisation and aspects to implementation. Int. J. Miner. Process., 119,
637 40-50.
638
639 Klauber, C., Gräfe, M. and Power, G., 2011. Bauxite residue issues: II. Options for residue
640 utilization. Hydrometallurgy 108, 11-32.
641
642 Kong, X., Guo, Y., Xue, S., Hartley, W., Wu, C., Ye, Y. and Cheng, Q., 2017a. Natural
643 evolution of alkaline characteristics in bauxite residue. J. Clean. Prod. 143, 224-230.
644
645 Kong, X., Li, M., Xue, S., Hartley, W., Chen, C., Wu, C., Li, X. and Li, Y., 2017b. Acid
646 transformation of bauxite residue: conversion of its alkaline characteristics. J. Hazard. Mat.
647 324, 382-390.
648
649 Kong, X., Tian, T., Xue, S., Hartley, W., Huang, L., Wu, C. and Li, C., 2018. Development of
650 alkaline electrochemical characteristics demonstrates soil formation in bauxite residue
651 undergoing natural rehabilitation. Land. Degrad. Dev 29, 58-67.
652
653 Liu, Y. and Naidu, R., 2014. Hidden values in bauxite residue (red mud): recovery of metals.
654 Waste Manage. 34, 2662-2673.
655
656 Menzies, N.W., Fulton, I.M., Kopittke, R.A. and Kopittke, P.M., 2009. Fresh water leaching
657 of alkaline bauxite residue after sea water neutralization. J. Environ. Qual. 38, 2050-2057.
658

McMahon, K. (2017) 'Bauxite Residue Disposal Area Rehabilitation', ISCOBA conference November 2017, Hamburg, 02-05 Oct, Hamburg, Germany. Available: http://icsoba.org/sites/default/files/2017papers/Bauxite%20Residue%20Papers/BR01%20-%20Bauxite%20Residue%20Disposal%20Area%20Rehabilitation.pdf [accessed: 21.02.2018].

Mohapatra, B.K., Mishra, B.K. and Mishra, C.R., 2012. Studies on metal flow from khondalite to bauxite to alumina and rejects from an alumina refinery, India. In Light Metals 2012 (87-91). Springer, Cham.

Morel, A., Borjon-Piron, Y., Porto, R.L., Brousse, T. and Bélanger, D., 2016. Suitable conditions for the use of vanadium nitride as an electrode for electrochemical capacitor. J. Electrochem. Soc. 163, A1077-A1082.

Nikbin, I.M., Aliaghazadeh, M., Charkhtab, S. and Fathollahpour, A., 2018. Environmental impacts and mechanical properties of lightweight concrete containing bauxite residue (red mud). J. Clean. Prod. 172, 2683-2694.

Petrakova, O.V., Panov, A.V., Gorbachev, S.N., Klimentenok, G.N., Perestoronin, A.V., Vishnyakov, S.E. and Anashkin, V.S., 2015. Improved efficiency of red mud processing through scandium oxide recovery. In Light Metals 2015 (93-96). Springer, Cham.

Pontikes, Y., Rathossi, C., Nikolopoulos, P., Angelopoulos, G.N., Jayaseelan, D.D. and Lee, W.E., 2009. Effect of firing temperature and atmosphere on sintering of ceramics made from Bayer process bauxite residue. Ceramics Internat. 35, 401-407.

Pontikes, Y. and Angelopoulos, G.N., 2013. Bauxite residue in cement and cementitious applications: current status and a possible way forward. Resourc. Conserv. Recycl 73, 53-63.

Power, G., Gräfe, M. and Klauber, C., 2011. Bauxite residue issues: I. current management, disposal and storage practices. Hydrometallurgy 108, 33-45.

Qin, S., Sun, Y., Li, Y., Wang, J., Zhao, C. and Gao, K., 2015. Coal deposits as promising alternative sources for gallium. Earth-Science Reviews 150, 95-101.

Qin, B. and Schneider, U., 2016. Catalytic use of elemental gallium for carbon–carbon bond formation. J.Am. Chem. Soc 138, 13119-13122.

Ricketts, N.J. and Duyvesteyn, W.P., 2018, March. Scandium recovery from the Nyngan laterite project in NSW. In TMS Annual Meeting & Exhibition (1539-1543). Springer, Cham.

Santini, T.C. and Fey, M.V., 2013. Spontaneous vegetation encroachment upon bauxite residue (red mud) as an indicator and facilitator of in situ remediation processes. Environ. Sci. Technol. 47, 12089-12096.

Tsakiridis, P.E., Agatzini-Leonardou, S. and Oustadakis, P., 2004. Red mud addition in the raw meal for the production of Portland cement clinker. J. Hazard. Mat. 116, 103-110.

Ujaczki, É., Klebercz, O., Feigl, V., Molnár, M., Magyar, Á., Uzinger, N. and Gruiz, K., 2015. Environmental toxicity assessment of the spilled Ajka red mud in soil microcosms for its potential utilisation as soil ameliorant. Periodica Polytechnica. Chem. Engin. 59, 253.

Ujaczki, É., Zimmermann, Y., Gasser, C., Molnár, M., Feigl, V. and Lenz, M., 2017. Red mud as secondary source for critical raw materials–purification of rare earth elements by liquid/liquid extraction. J. Chem. Technol. Biotech. 92, 2835-2844.

Ujaczki, É., Feigl, V., Molnár, M., Cusack, P., Curtin, T., Courtney, R., O'Donoghue, L., Davris, P., Hugi, C., Evangelou, M.W. and Balomenos, E., 2018. Re-using bauxite residues: benefits beyond (critical raw) material recovery. J. Chem. Technol. Biotech 93, 2498-2510.

United States Geological Survey Website (USGS). Commodity Statisctics and Information (2016). Available: http://minerals.usgs.gov/minerals/pubs/commodity/ [accessed 30.01.2018].

Wang, S., Ang, H.M. and Tade, M.O., 2008. Novel applications of red mud as coagulant, adsorbent and catalyst for environmentally benign processes. Chemosphere 72, 1621-1635.

Wang, W., Pranolo, Y. and Cheng, C.Y., 2013. Recovery of scandium from synthetic red mud leach solutions by solvent extraction with D2EHPA. Sep.Purif. Technol 108, 96-102.

Wang, X., Zhang, Y., Lv, F., An, Q., Lu, R., Hu, P. and Jiang, S., 2015. Removal of alkali in the red mud by SO2 and simulated flue gas under mild conditions. Environ. Prog. Sustain. Ener. 34, 81-87.

732 Weng, Z., Jowitt, S.M., Mudd, G.M. and Haque, N., 2015. A detailed assessment of global rare
733 earth element resources: opportunities and challenges. Econ. Geol. 110, 1925-1952.
734
735 Xu, C., Kynický, J., Smith, M.P., Kopriva, A., Brtnický, M., Urubek, T., Yang, Y., Zhao, Z.,
736 He, C. and Song, W., 2017. Origin of heavy rare earth mineralization in South China. Nature
737 Comm. 8, 14598.
738
739 Xue, S., Kong, X., Zhu, F., Hartley, W., Li, X. and Li, Y., 2016. Proposal for management and
740 alkalinity transformation of bauxite residue in China. Environ. Sci. Poll. Res. 23, 12822-12834.
741
742 Xue, S., Li, M., Jiang, J., Millar, G.J., Li, C. and Kong, X., 2018. Phosphogypsum
743 stabilization of bauxite residue: conversion of its alkaline characteristics. J. Environ. Sci.
744 https://doi.org/10.1016/j.jes.2018.05.016
745
746 Zhu, F., Liao, J., Xue, S., Hartley, W., Zou, Q. and Wu, H., 2016. Evaluation of aggregate
747 microstructures following natural regeneration in bauxite residue as characterized by
748 synchrotron-based X-ray micro-computed tomography. Sci. Tot. Environ. 573, 155-163.
749
750 Zhu, F., Xue, S., Hartley, W., Huang, L., Wu, C. and Li, X., 2016. Novel predictors of soil
751 genesis following natural weathering processes of bauxite residues. Environ. Sci. Poll. Res. 23,
752 2856-2863.
753
754 Zhu, F., Cheng, Q., Xue, S., Li, C., Hartley, W., Wu, C. and Tian, T., 2018. Influence of natural
755 regeneration on fractal features of residue microaggregates in bauxite residue disposal areas.
756 Land Degrad. Dev. 29, 138-149.

Table 1 Sample information regarding the year of production for each of the bauxite residue samples over a twelve-year period. The sample code for each bauxite residue sample is also included in the table.

Sample Code	Sample Description	Year of Disposal
BR 12	Bauxite Residue	2004
BR 11	Bauxite Residue	2005
BR 10	Bauxite Residue	2006
BR 9	Bauxite Residue	2007
BR 8	Bauxite Residue	2008
BR 7	Bauxite Residue	2009
BR 6	Bauxite Residue	2010
BR 5	Bauxite Residue	2011
BR 4	Bauxite Residue	2012
BR 3	Bauxite Residue	2013
BR 2	Bauxite Residue	2014
BR 1	Bauxite Residue	2015

Table 2 Physico-chemical composition of the bauxite residue mud over a twelve-year storage period, inclusive of pH, EC, moisture content, bulk density and particle size distribution.

Sample	pH	EC (mS cm^{-1})	Moisture content (%)	Bulk density (g cm^{-3})	d_{10} (µm)[a]	d_{50} (µm)[b]	d_{90} (µm)[c]
BR 12	11.6 ± 0.02	1.0 ± 0.01	26.8 ± 0.7	1.4 ± 0.04	0.7 ± 0.1	2.6 ± 0.1	7.0 ± 1.2
BR 11	10.8 ± 0.1	0.4 ± 0.02	28.2 ± 0.7	1.3 ± 0.03	0.9 ± 0.1	3.5 ± 0.5	9.6 ± 0.5
BR 10	12.0 ± 0.02	3.3 ± 0.2	26.8 ± 0.1	1.4 ± 0.1	1.4 ± 0.1	4.0 ± 0.3	12.3 ± 1.6
BR 9	10.0 ± 0.1	0.4 ± 0.01	24.3 ± 0.3	1.1 ± 0.1	1.0 ± 0.1	4.3 ± 0.4	12.4 ± 1.0
BR 8	11.4 ± 0.1	1.0 ± 0.1	27.2 ± 0.3	1.4 ± 0.1	0.8 ± 0.1	2.6 ± 0.1	6.8 ± 0.2
BR 7	10.4 ± 0.02	0.5 ± 0.01	22.3 ± 0.6	1.4 ± 0.04	0.9 ± 0.2	3.2 ± 0.5	12.7 ± 2.7
BR 6	10.7 ± 0.03	0.5 ± 0.03	25.8 ± 1.0	1.3 ± 0.04	0.7 ± 0.1	2.6 ± 0.01	6.7 ± 0.2
BR 5	10.3 ± 0.1	0.4 ± 0.03	22.0 ± 0.5	1.2 ± 0.1	0.6 ± 0.01	2.4 ± 0.04	7.9 ± 1.1
BR 4	11.5 ± 0.1	0.9 ± 0.02	31.1 ± 0.5	1.3 ± 0.1	1.2 ± 0.1	3.8 ± 0.6	12.70 ± 2.3
BR 3	10.6 ± 0.02	0.5 ± 0.01	23.8 ± 0.3	1.3 ± 0.03	0.8 ± 0.2	2.6 ± 0.3	8.3 ± 1.6
BR 2	11.2 ± 0.01	0.9 ± 0.02	28.1 ± 1.9	1.3 ± 0.1	1.1 ± 0.02	3.2 ± 0.02	9.7 ± 0.9
BR 1	10.3 ± 0.1	0.7 ± 0.03	25.0 ± 2.7	1.5 ± 0.02	0.5 ± 0.01	2.2 ± 0.1	6.7 ± 0.6

[a]d_{10} (µm) = the size of particles at 10% of the total particle distribution.
[b]d_{50} (µm) = the median; the size of particles at 50% of the total particle distribution.
[c]d_{90} (µm) = the size of particles at 90% of the total particle distribution.

Table 3 Main mineralogical composition (%) of the bauxite residue samples taken from the BRDA ranging from one to twelve years old, as determined by XRF.

Code	Al_2O_3	Fe_2O	SiO_2	TiO_2	CaO
BR 11	17.0±0.61	42.0±1.20	9.82±0.32	9.41±0.34	6.03±0.79
BR 10	17.1±0.4	41.5±0.96	10.2±0.56	9.52±0.6	6.03±0.49
BR 9	17.8±0.73	40.1±1.40	10.9±0.47	8.97±0.51	6.04±0.4
BR 8	16.8±0.58	41.8±1.40	9.89±0.39	9.41±0.61	5.97±0.49
BR 7	14.8±1.5	47.5±2.0	7.20±1.0	10.3±0.95	6.1±1.0
BR 6	16.2±0.54	45.9±2.10	8.0±0.57	9.54±0.78	5.70±0.66
BR 5	16.2±0.66	44.4±1.30	9.35±0.60	8.62±0.71	5.75±0.53
BR 4	16.5±0.65	43.3±1.20	9.38±0.53	8.91±0.53	6.21±0.35
BR 3	15.8±0.45	44.3±1.90	8.85±0.47	9.18±0.62	6.34±0.35
BR 2	16.0±0.71	46.6±1.80	8.95±0.70	8.21±0.38	5.0±0.40
BR 1	16.2±0.6	46.8±1.61	8.76±0.48	8.33±0.56	4.69±0.43

807

808

809

810

811 **Table 4** CRM composition (in mg kg^{-1}) of the bauxite residue samples, taken from the BRDA, as detected on ICP-OES following aqua regia digestion.

Element	BR 12	BR 11	BR 10	BR 9	BR 8	BR 7	BR 6	BR 5	BR 4	BR 3	BR 2
Dy	3.6 ± 0.02	5.4 ± 0.01	7.19 ± 0.01	5.39 ± 0.001	5.4 ± 0.04	5.39 ± 0.01	5.4 ± 0.01	5.38 ± 0.02	4.51 ± 1.3	7.2 ± 0.002	5.4 ± 0.02
Er	4.8 ± 0.5	5.4 ± 0.01	5.7 ± 0.5	4.94 ± 0.6	5.4 ± 0.04	5.39 ± 0.01	4.49 ± 0.01	5.38 ± 0.01	4.05± 0.6	5.4 ± 0.001	5.4 ± 0.02
Lu	8.39 ± 0.5	7.8 ± 0.5	8.09 ± 0.01	7.49 ± 0.5	8.1 ± 0.05	7.63 ± 0.6	8.1 ± 0.02	8.37 ± 0.5	7.66±0.7	8.1 ± 0.002	8.09 ± 0.03
Y	35.6 ± 3.2	39.8 ± 1.2	44.4 ± 1.5	41.9 ± 1.5	42 ± 0.4	39.5 ± 0.04	33.4 ± 0.4	41 ± 2.0	36.9± 1.4	47.4 ± 1.2	39.3 ± 0.5
Yb	8.39 ± 0.6	8.8 ± 0.3	9.39 ± 0.3	8.79 ± 0.7	9.4 ± 0.3	8.68 ± 0.4	8.2 ± 0.4	8.97 ± 0.9	8.11± 0.4	9.6 ± 0.002	8.71 ± 0.4
Ce	126 ± 10.1	126 ± 3.5	156 ± 2.2	136 ± 7.6	157 ± 2.2	128 ± 3.3	146 ± 6.7	200 ± 8.4	102± 3.5	147 ± 4.2	139 ± 6.8
Eu	2.40 ± 0.01	2.40 ± 0.01	2.40 ± 0.005	2.40 ± 0.01	2.40 ± 0.02	2.39 ± 0.003	2.40 ± 0.01	3.59 ± 0.01	2.40± 0.01	2.40 ± 0.001	2.40 ± 0.005
Gd	6.75 ± 0.6	6.60 ± 0.5	7.64 ± 0.6	7.63 ± 0.6	9.30 ± 0.6	7.18 ± 1.3	6.75 ± 0.6	8.98 ± 0.02	5.41± 0.02	9 ± 0.002	6.73 ± 0.6
La	91.3 ± 8.6	88.2 ± 3.2	108 ± 2.3	94.1 ± 2.7	106.4 ±1.0	89.2 ± 0.9	104 ± 3.5	134 ± 4.4	68.8± 4.0	98.2 ± 2.1	91± 2.4
Nd	80.1 ± 7.4	77.2 ± 5.3	93.9 ± 6.5	84.7 ± 1.3	98 ± 5.3	85.6 ± 8.6	88.9 ± 8.6	118 ± 4.4	64.6± 4.0	93 ± 2.2	94.3 ± 11.3
Pr	41.1 ± 3.5	42.9 ± 4.2	47.7 ± 3.3	42.5 ± 3.1	50.1 ± 1.6	40.8 ± 1.9	45 ± 2.7	56.2 ± 5.3	34.7± 3.3	45 ± 0.9	42.3 ± 1.1
Sc	50.2 ± 4.1	50.4 ± 1.6	60.2 ± 2.2	56.1 ± 2.7	54.2 ± 0.9	55.7 ± 1.3	45.4 ± 0.2	56 ± 4.2	42.9± 2.3	49 ± 1.3	45.6 ± 4.3
Sm	19.3 ± 0.7	20.7 ± 1.8	21 ± 2.2	21.6 ± 0.9	21.6 ± 0.8	18.4 ± 1.9	21.6 ± 0.9	25.1 ± 0.05	18± 1.2	21 ± 1.0	20.3 ± 2.0

Co	8.69 ± 0.5	7.64 ± 0.6	7.79 ± 0.5	6.73 ± 0.6	8.10 ± 0.05	7.63 ± 0.6	6.6 ± 0.5	8.67 ± 0.5	7.21 ± 0.02	8.4 ± 0.5	7.49 ± 0.6
Ga	107 ± 8.5	112 ± 2.3	102 ± 0.7	114 ± 5.2	98.6 ± 0.2	113 ± 3.8	106 ± 2.7	114 ± 5.1	99.5 ± 1.8	114 ± 1.9	94.4 ± 2.7
In	30.1 ± 1.8	34.6 ± 0.7	31.5 ± 1.5	32.1 ± 2.7	36.9 ± 0.9	30.5 ± 1.3	29.2 ± 2	33.6 ± 0.7	28.4 ± 0.7	34.5 ± 7.2	36.4 ± 4.3
Mo	3.14 ± 0.6	4.49 ± 0.01	4.04 ± 0.6	4.95 ± 0.6	4.48 ±0.004	4.95 ± 0.6	4.49 ± 0.01	4.48 ± 0.01	4.94 ± 1.9	4.8 ± 0.5	4.48± 0.01
V	593 ± 60.6	419 ± 8.2	596 ± 19.8	439 ± 41.1	491 ± 20.3	445 ± 41.2	484 ± 48.2	600 ± 24.3	401 ± 41.2	571 ± 13.3	573 ± 41.1

812

Table 5 Associated financial value of economically interesting elements in the bauxite residue (average over a twelve-year period, n = 11).

Element	Average aqua regia extracted content (mg kg^{-1})	Price* (US \$ t^{-1})	Economic value of the bauxite residue in this study*** (US \$ t^{-1})
Ga	107±7.3	400,000	42.73
Sc	51.4±5.4	4,600,000	236.44
In	32.5±2.9	240,000	7.81
V	510±77.8	6,889	3.51
Nd	89.0±13.6	39,500	3.51
Dy	5.48±1.0	184,500	1.01
Pr	44.4±5.6	5,500**	0.24
Y	40.1±3.9	35,500	1.42
Ce	142±24.9	2,000	0.28
Sm	20.8±1.9	12,500**	0.26
Co	7.72±0.7	26,444	0.20
La	97.5±16.3	2,000	0.19
Eu	2.51±0.4	66,000	0.16
Yb	8.82±0.5	5,500**	0.04
Lu	7.99±0.3	5,500**	0.04
Gd	7.45±1.2	5,500**	0.04
Mo	4.48±0.5	14,500	0.06
Er	5.12±0.5	5,500**	0.03

*Values from USGS (2016)
**Average value for mischmetals of REE/expected higher individual prices
*** Economic value of the bauxite residue in this study, determined using current price (US \$ t^{-1}) and the average content in the bauxite residue studied.

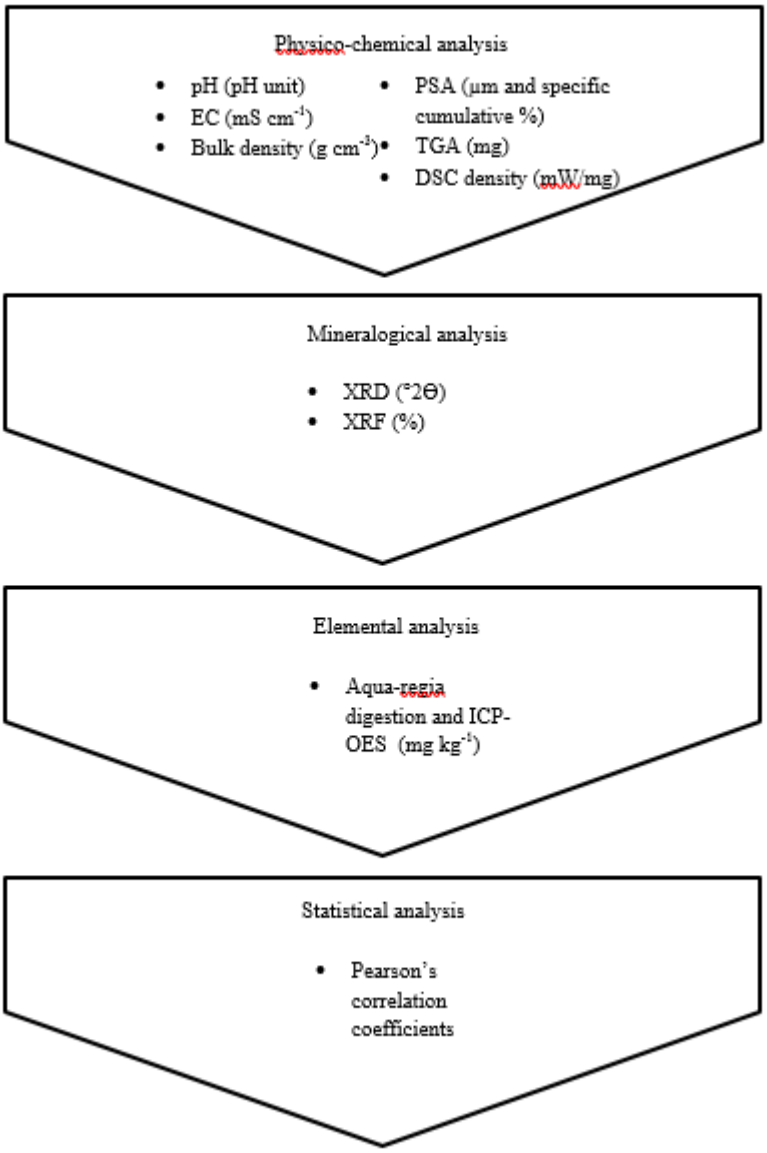

828

829

830 **Figure 1** Flow chart illustrating the experimental analysis carried out on the bauxite residue samples
831 obtained. Once obtained from the BRDA, the bauxite residue was analysed for its main physico-
832 chemical analysis (pH, EC, bulk density, PSA, TGA and DSC), mineralogical analysis (XRD and
833 XRF), and elemental analysis (measure using ICP-OES following aqua-regia digestion). Once all
834 data was obtained, statistical analysis was carried out using Pearson's correlation coefficients.
835
836

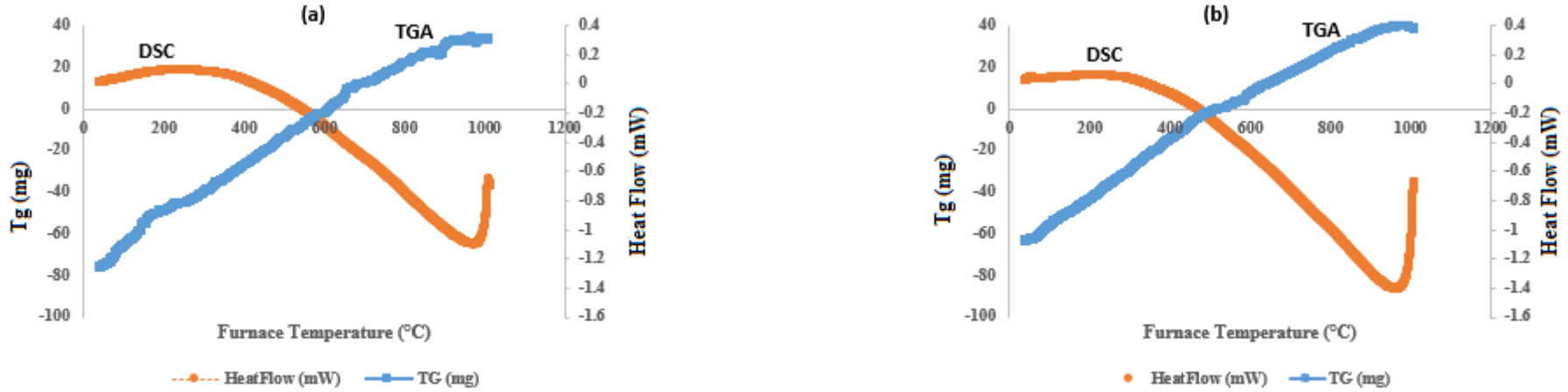

837 **Figure 2** TGA (descending) / DSC (ascending) curve obtained for bauxite residue (a) BR12 (2004) and (b) BR2 (2014). Remaining TGA / DSC graphs

838 found in Figure S4. The TGA curves showed weight loss between 300 and 975 °C for all the bauxite residues examined.

839